High-Yield Single-Walled Carbon Nanotubes Synthesized on the Small-Pore (C10) Co-MCM-41 Catalyst

Sangyun Lim,[†] Nan Li,[‡] Fang Fang,[‡] Mathieu Pinault,[§] Codruta Zoican,[‡] Chuan Wang,[‡] Tarek Fadel,[||] Lisa D. Pfefferle,[‡] and Gary L. Haller*[,‡]

Chevron Phillips Chemical Company, 1862 Kingwood Drive, Kingwood, Texas 77339, Department of Chemical Engineering, Yale University, P.O. Box 208286, New Haven, Connecticut 06520-8286, CEA Saclay, DSM/DRECAM/SPAM, Laboratoire Francis Perrin, Bât. 522, P. 249A, 91191 Gif sur Yvette Cedex, France, and Department of Biomedical Engineering, Yale University, P.O. Box 208284, New Haven, Connecticut 06520-8284

Received: November 12, 2007; Revised Manuscript Received: March 14, 2008

High-quality single-walled carbon nanotubes (SWNT) with high yield were produced by using small-pore Co-MCM-41 catalyst, templated by a C10 surfactant and containing 3 wt % Co. A complete incorporation of Co ions in the silica matrix without formation of surface Co oxides and the contact time of the reaction, in the catalyst synthesis and the SWNT production, respectively, were the most critical factors to be considered. By controlling the reduction temperature and contact time in the reaction, the carbon yield could reach 34 wt % or higher with a selectivity of 96 wt % to SWNT. The metal content after purification of SWNT by base−acid treatments was 0.7 wt %, and the surface area was as high as 1800 m^2/g. The metal surface occlusion effect by amorphous silica might play a key role in the stabilization of the completely reduced Co metallic clusters in the SWNT synthesis procedure, using small-pore C10 Co-MCM-41.

Introduction

The catalytic growth of carbon single-walled nanotubes (SWNT) by decomposition of carbon-containing molecules over a metal catalyst is a promising technique for scaling up the nanotube production process.[1] This is required for applications that require larger quantities of SWNT with a quality and purity that exceeds that achieved by arc discharge or laser ablation methods. Many successful solid catalytic processes for the synthesis of high-quality SWNT have been reported. In particular, narrow tube diameter distributions have been demonstrated by using CO disproportionation on Co-Mo/SiO_2[2] and Co-MCM-41 catalyts.[3] These processes exhibit high selectivity to SWNT (>90−95 wt %) in the carbon product with low defect density and a narrow tube size distribution, attractive for many applications of SWNT. There are many factors affecting SWNT quality and yield in the catalytic process: reaction temperature, pressure, reactor flow velocity, pretreatment of catalyst, etc. SWNT yield and quality are directly related to these factors, which can be improved by a systematic investigation of both catalyst and reaction conditions that have not been critically examined previously. Yield of SWNT in a high area (porous) solid catalytic process, especially, has been a major barrier to productivity that is not easily overcome. Yields of SWNT of 5−6 wt % on high area supported catalysts are typical. Although there have been several reports of super yields of SWNT with use of a nonsolid catalytic process, very low surface area (nonporous) catalysts, or different carbon sources (other than CO), the quality of the SWNT produced (tube size distribution and chirality control) remains unclear.[4–6] High SWNT yield with use of a high area solid catalytic process, therefore, could be a significant benefit in a scaled-up process for a stable supply of high-quality SWNT.

Previously, the effect of reaction factors and catalyst pretreatment on the SWNT quality and yield in the solid catalytic process has been thoroughly investigated.[7,8] The catalytic system used was C16 Co-MCM-41 having a pore diameter of about 2.9 nm measured by the BJH method.[9] This catalyst contains <5 wt % surface Co oxides, which lower the reduction stability of Co ions in the framework by a hydrogen spillover effect on the surface.[10] This may cause aggregation of metallic clusters at relatively mild temperatures, producing unwanted carbon species, i.e., graphite, resulting in limited SWNT carbon yield because SWNT cannot grow once the metallic particles are covered by graphite.

The C10 MCM-41 having a pore diameter of 1.8 nm measured by the BJH method can accommodate more Co ions in the silica matrix without formation of surface oxides than is the case for C16 MCM-41. The reduction stability of C10 Co-MCM-41 is much higher than that of C16 Co-MCM-41 and exhibits a very narrow temperature range for full reduction. Because of the faster cation migration at higher temperature, most Co ions can be utilized for SWNT production, resulting in a high yield. We demonstrate that these properties of C10 Co-MCM-41, with modification of the reaction and pretreatment conditions, can significantly improve carbon yield.

In this study, the C10 3 wt % Co-MCM-41 samples were synthesized from different soluble and colloidal silica ratios, and the initial pH of the synthesis solution, a variable previously studied in the C16 catalysts.[11,12] The physical properties were measured by nitrogen physisorption, showing the volume-averaged structure indices,[13] and the chemical properties were investigated by hydrogen temperature-programmed reduction (TPR) and in situ X-ray absorption spectroscopy (EXAFS). The C10 Co-MCM-41 catalysts are used for the synthesis of SWNT,

* To whom correspondence should be addressed. E-mail: gary.haller@yale.edu. Phone: 203-432-4378. Fax: 203-432-4387.
[†] Chevron Phillips Chemical Company.
[‡] Department of Chemical Engineering, Yale University.
[§] CEA Saclay, DSM/DRECAM/SPAM, Laboratoire Francis Perrin.
[||] Department of Biomedical Engineering, Yale University.

10.1021/jp710805u CCC: $40.75
Published on Web 07/19/2008

using CO disproportionation to monitor catalytic behavior by comparing SWNT yield and characteristics measured by Raman spectroscopy and temperature-programmed oxidation (TPO) with TG/DTG. Finally, the data collected will be analyzed to suggest a preliminary mechanism explaining the relationship between catalytic properties and high SWNT yield.

Experimental Section

Catalyst Preparation. The silica synthesis sources used were Cab-O-Sil M-5 from Sigma-Aldrich, colloidal silica, and tetramethyl ammonium silicate (TMASi, 10 wt % silica, TMA/Si mol ratio = 0.75, SACHEM, Inc.), and soluble silica. The Co source was $CoSO_4 \cdot 7H_2O$ (Sigma-Aldrich). The quaternary ammonium surfactants $C_nH_{2n+1}(CH_3)_3NBr$ were purchased from Aldrich Co. with $n = 16$ and from American Tokyo Kasei with $n = 10$. The surfactant solutions were prepared by ion-exchanging the 29 wt % (C10), 20 wt % (C16) of $C_nH_{2n+1}(CH_3)_3NBr$ aqueous solution with a 40% molar excess exchange capacity of Amberjet-400 (OH) ion-exchange resin (Sigma-Aldrich) by overnight batch mixing. The antifoaming agent was Antifoam A from Sigma-Aldrich, a silane polymer alkyl terminated by methoxy groups. Acetic acid (Fisher Scientific) was used for pH adjustment of the synthesis solution. Hereafter, specific samples are designated by the alkyl chain length of the surfactant used (e.g., C10 Co-MCM-41).

Cab-O-Sil M-5, TMASi, and the $CoSO_4 \cdot 7H_2O$ aqueous solution were mixed for 30 min. The silica ratio between soluble silica and total silica was varied from 0.14 to 0.70 to investigate the TMASi effect on the physicochemical properties of Co-MCM-41. The surfactant solution was added to the prepared silica and Co mixture, and a small amount of antifoaming agent (0.2 wt % of surfactant) was incorporated to remove excess foam produced by the surfactant as a result of vigorous stirring. Acetic acid was added to adjust the pH of the synthesis solution from 12.5 to 10.5. After additional mixing over 30 min, this synthesis solution was transferred into a 250 mL polypropylene bottle and placed in an autoclave at 100 °C for 6 days. After cooling to room temperature, the resulting solid was recovered by filtration, washed with deionized water, and dried under ambient conditions. The predried solid was heated from room temperature to 540 °C over 17 h under flowing He (30 mL/(min·g solid)) and soaked for 1 h at 540 °C in flowing He followed by calcination for 5 h at 540 °C under flowing air to remove the residual organics. The molar ratio of each component in the synthesis solution was controlled at SiO_2:surfactant:Co:H_2O = 1:0.27:0.01 or 0.03:86. Because the preparation process may cause some loss of Co and silica in the byproduct, the final Co content of each sample was determined by ICP at Galbraith Laboratory Inc. and confirmed by X-ray absorption spectroscopy (XAS) at NSLS, Brookhaven National Laboratory.

Catalyst Characterization. Nitrogen adsorption−desorption isotherms were measured at −196 °C with a static volumetric instrument Autosorb-3B (Quantachrome). Prior to the measurement, the samples were outgassed at 300 °C to a residual pressure below 1×10^{-4} Torr. A Baratron pressure transducer (0.001−10 Torr) was used for low-pressure measurements. The pore size distributions were calculated from the desorption isotherms by using the BJH method.[9] Although the BJH method underestimates the mesopore size, the pore size distribution determined in our study provides reliable results that can be used for the relative comparison of the synthesized samples.

The reduction stability of the Co-MCM-41 samples was investigated by a hydrogen temperature-programmed reduction (TPR) technique, using the thermal conductivity detector (TCD) of a gas chromatograph (6890 plus, Agilent). Approximately 200 mg of each sample was loaded into a quartz cell. Prior to each TPR run, the sample cell was purged by ultra zero grade air at room temperature, then the temperature was increased to 500 °C at 5 °C/min, soaked for 1 h at the same temperature, and cooled to room temperature. This procedure produces a clean surface with a uniform degree of dehydration before running the TPR. The gas flow was switched to 5% hydrogen in argon balance, and the baseline was monitored until stable. After baseline stabilization, the sample cell was heated at 5 °C/min to 850 °C and held for 1 h at the same temperature to ensure complete cobalt reduction. A dry ice acetone trap was installed between the sample cell and the TCD to condense water, produced by sample reduction.

As a complementary experiment to TPR and for the measurement of the metallic Co cluster size, in situ and ex situ X-ray absorption experiments were performed at the Co K edge (7709 eV) with Si (111) as the monochromator crystal at station X23A2 in the NSLS, 2.5 GeV storage ring, Brookhaven National Laboratory. Eighty milligrams of each sample was pressed into a self-supporting wafer and placed in a stainless steel cell equipped with beryllium (0.5 mm thick, Aldrich) windows, gas inlet and outlet, liquid nitrogen cooling line, and heating elements allowing in situ controlled atmosphere treatments up to 750 °C. To characterize the effect of the reduction temperature, each sample was reduced at 700 °C by flowing ultrahigh purity hydrogen for 30 min and quenched at 0 °C by using the liquid nitrogen cooling line. Extended X-ray absorption fine structure (EXAFS) spectra were recorded for the measurement of Co cluster sizes of samples after each sample treatment described above. The spectra collected were analyzed with use of the UWXAFS analysis package.[14]

CO Disproportionation. SWNT were synthesized by CO disproportionation. For a typical batch, 200 mg of fresh Co-MCM-41 was loaded into an 18 mm internal diameter quartz reactor placed in Omega ceramic fiber radiant heater, which allows precise temperature control throughout the catalyst bed. Prior to exposure to pure CO (filtered of residual metal−carbonyls by thermal decomposition before entering the reactor), the catalyst was heated in flowing hydrogen at 1 atm at 20 °C/min from room temperature to a desired reduction temperature in the range from 650 to 850 °C and reduced isothermally for 30 min. After the prereduction, the catalyst was purged with ultrahigh purity argon at the reduction temperature, and then heated from the reduction temperature to the desired reaction temperature at 20 °C/min in flowing argon or held at the same temperature if the reaction was performed at the reduction temperature. SWNT were grown for 60 min at different temperatures ranging from 700 to 850 °C under 6 atm of CO. To investigate the contact time effect on the SWNT yield, the catalyst amount was altered from 30 mg to 500 mg under the same CO flow rate (1 L/min). For the investigation of the linear velocity effect on the carbon yield, the CO flow rate was changed in the range from 1 to 2 L/min, using a fixed amount of catalyst and reactor diameter.

Carbon Characterization. To obtain total carbon yield and SWNT selectivity, thermal gravimetric analysis (TGA) data of carbon oxidation were collected in a Setaram Setsys 1750 instrument under air flow. Samples of carbon-deposited catalysts were held at 150 °C for 1 h for dehydration before the temperature program. The weight change in the sample was monitored over the temperature program from 150 to 1000 °C at 10 °C/min for two successive ramps; the second was used as

TABLE 1: Physical Properties of the Co-MCM-41 Samples Obtained from Nitrogen Physisorption

catalyst	Co loading (wt %)	initial pH	Si from TMASi/total SiO_2	BET area (m^2/g)	pore diameter[a] (Å)	slope[b] (cm^3/g)	mesopore vol[c] (cm^3/g)
C10 Co-MCM-41	1	11.5	0.14	828.8	18.9	932	0.39
	1	11.5	0.29	1247	18.4	1745	0.68
	1	11.5	0.43	1290	18.4	1833	0.70
	1	11.5	0.57	1588	17.8	1716	0.72
	1	11.5	0.70	1849	16.6	1691	0.80
	3	10.5	0.43	840.1	18.9	910	0.43
	3	11.0	0.43	828.6	18.9	1048	0.46
	3	11.5	0.43	1212	18.9	1563	0.66
	3	12.0	0.43	1293	18.4	1672	0.66
	3	12.5	0.43	1438	17.8	1529	0.66
C16 Co-MCM-41	3	11.5	0.29	1294	28.6	5320	1.12

[a] Calculated by the BJH method. [b] Slope of the capillary condensation of isotherm. [c] Defined as pores having smaller diameter than 100 Å.

a baseline correction for the first. A special holey alumina crucible was used to limit mass transfer interference.

Raman spectra of the as-synthesized SWNT without any purification or pretreatment were recorded with excitation wavelengths of 532 and 785 nm on a NRS-3100 instrument from Jasco equipped with a con-focal microscope.

High-resolution transmission electron microscopic (HR-TEM) images were recorded on a Philips Tecnai F20 TEM instrument equipped with a field emission gun and accelerating voltages of 200 kV. The point resolution and the line resolution were 0.24 and 0.12 nm, respectively, at a focal length of 1.7 mm. Samples were prepared by ultrasonicating about 1 mg of the sample in 10 mL of ethanol (ACS/USP grade). A drop of this suspension was then applied on a lacey carbon-coated copper TEM grid and dried before the experiment.

Results and Discussion

Characteristics of C10 Co-MCM-41. Silica sources used in this study are colloidal silica (Cab-O-Sil) and soluble silica (TMASi). The soluble silica (organic silica) was used as a digesting agent for colloidal silica instead of NaOH to avoid the negative effect of Na cations on metal ion incorporation and catalytic activity.[15] There are many synthesis factors affecting the physical and chemical properties of the final product of metal ion incorporated MCM-41; TMASi is one of those factors previously investigated on C16 Co-MCM-41, Ni-MCM-41, and V-MCM-41.[13] At high soluble silica concentration, metal ion incorporated MCM-41 showed a property of silicate-like material having smaller pore size, resulting in higher surface area per unit mass. However, the structure of MCM-41 deteriorated as a function of the amount of soluble silica used beyond an optimum value. A low concentration of soluble silica also gives a low-quality MCM-41 structure because the gel contains insufficient organic base to digest colloidal silica.[16] By the nitrogen physisorption analysis, a similar effect of soluble silica on C10 Co-MCM-41 catalyst structure was observed, as shown in Table 1. The silica ratio between soluble silica and total silica was varied from 0.14 to 0.70 to select the optimum C10 Co-MCM-41 catalyst structure. Unlike C16 Co-MCM-41, where the optimum ratio was 0.29 between soluble and total silica, C10 Co-MCM-41 shows the highest slope of capillary condensation at a ratio of 0.43. At higher ratio than this, pore size starts to decrease, resulting in greater surface area with degrading structure. At a ratio below 0.43, there are no significant pore size differences; however, surface area and mesopore volume are decreased. The structural deterioration of C10 Co-MCM-41 catalysts at low and high soluble to total silica ratio was clearly observed in the adsorption−desorption isotherms (not shown here) of these samples by showing hysteresis loops. In this study, therefore, all C10 Co-MCM-41 catalysts used for SWNT synthesis are synthesized by using a soluable/total silica ratio of 0.43.

Previously, it has been shown that the distribution of Co ions in the silica matrix could be controlled by the initial pH adjustment of the C16 Co-MCM-41 synthesis solution.[12] In this study, the same effect was investigated with C10 Co-MCM-41 (3 wt % Co) catalysts synthesized with different silica ratio between soluble and total silica (0.43). Table 1 indicates that surface area is increased as a function of pH, suggesting that the catalyst becomes more porous at high pH. However, the increase of surface area at pH 12 and 12.5 may be caused by the decrease of pore size. The highest structural order was obtained at pH 12 with the greatest mesopore volume, indicating an optimum structure. Higher pH than this may damage the structure because of the excess porosity, as explained earlier.[12] When this optimized C10 Co-MCM-41 was compared to the optimized C16 Co-MCM-41, obtained previously,[17] the slope of capillary condensation and mesopore volume of the C10 sample show much lower values than those of C16, which may be related to the lower hydrophobicity of the C10 surfactant than that of C16. That is, micelle creation and stability of the C10 surfactant in the aqueous solution is less favorable than for longer chain length surfactant, resulting in a low degree of long-range order of pore structure and a low yield of mesopore structure, directly related to the slope of capillary condensation and mesopore volume, respectively.

The reduction stability of C10 Co-MCM-41 catalysts was investigated by TPR, as described earlier, and the results are depicted in Figure 1. The reduction temperature at the maximum rate shifts as a function of the initial pH because more Co metal ions are distributed inside the silica matrix at higher pH, as explained in an earlier report.[12] More distinctive features of these C10 samples are the narrow and intense reduction pattern without surface compounds (low-temperataure reduction peaks), compared to C16 Co-MCM-41. The surface compounds (oxides) form large metallic particles by unconstrained migration on the pore wall surface (and out of the pores) under the continuous reduction conditions, resulting in the formation of unwanted carbon species and low SWNT yield. There are no surface oxides, resulting from unincorporated Co cations in the silica matrix in C10 Co-MCM-41 samples regardless of the initial pH. The narrow reduction temperature range can be a benefit to maximize the effectiveness of Co for the synthesis of SWNT. Because more Co can be utilized at a fixed reduction and reaction temperature, this will result in higher yield if the particle size can be controlled by anchoring the particles at this high

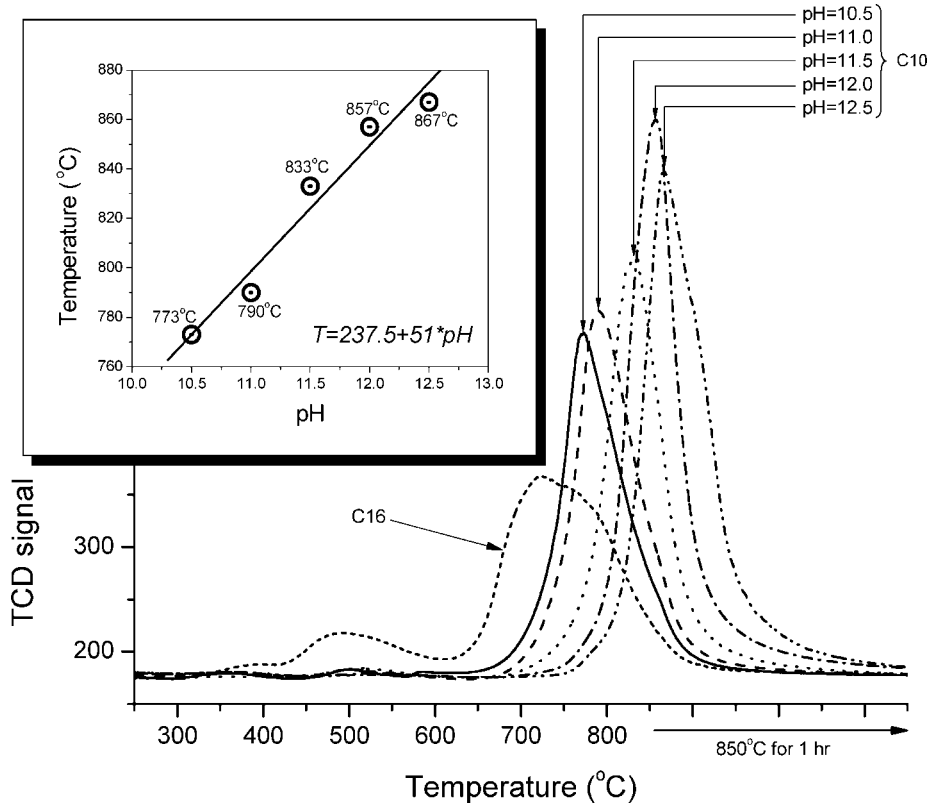

Figure 1. Temperature-programmed reduction (TPR) results of C10 3 wt % Co-MCM-41 catalysts synthesized under the different initial pH of the synthesis solution.

temperature. A broad reduction temperature range, as exhibited by the C16 sample, can only utilize a small portion of the Co that can be reduced only at a certain fixed temperature. Therefore, the catalytic performance in SWNT synthesis was expected to be improved with C10 Co-MCM-41 catalysts compared to C16 Co-MCM-41.

The edge step of the X-ray absorption spectrum can be used as an accurate measurement of atomic concentration in the sample. The physical meaning of the edge step is the change in the absorption coefficient at the edge energy of an atom, which is directly related to the atom concentration, as shown in Figure 2a. Figure 2b shows the relationship of Co concentration of C10 Co-MCM-41 samples prepared under different initial pH measured by chemical analysis (ICP) and X-ray absorption analysis. By this comparison, the experimental error of chemical analysis can be easily found and corrected, as shown in Figure 2b. To prove this interpretation, the peak area of TPR obtained from each sample having different initial pH (from Figure 1) was compared to the edge step, as shown in Figure 2c. The TPR peak area corresponds to the hydrogen consumption during the reduction of Co metal ions, which is a useful technique for quantification of a single reducible ion. Unlike chemical analysis, the TPR peak area shows a linear correlation with the edge step, which demonstrates that metal ion concentration can be accurately obtained by using the XANES experiment. This also suggests that XANES is a useful technique for checking the reliability of other quantification results. Cobalt concentration is linearly increased as a function of the initial pH. Although higher pH produces a higher concentration of Co, it does not seem to result in more incorporation of Co in the silica matrix. Rather, it appears that a lower yield of silica occurs at high pH than more substitution of silicon ions by Co ions because all the chemical compositions were fixed in the synthesis of these samples (3 wt % of Co) and the final Co concentrations are more than 3 wt % at pH >12 (3 wt % Co being the synthesis composition).

As a complementary experiment of TPR, X-ray absorption spectra of fresh and partially reduced C10 Co-MCM-41 samples were collected at X23A2, NSLS, Brookhaven National Laboratory. The in situ partial reduction was performed in a stainless steel chamber under flowing hydrogen at 700 °C for 30 min before collecting spectra. For comparison of the coordination number of Co with surrounding oxygen anions and bond length, $CoAl_2O_4$ was selected as a reference sample having tetrahedral local coordination of Co with surrounding oxygen ions. Collected data were analyzed by using the Kaiser−Bessel function in the range of $k = 2.5-12$ and $R = 1-3$, $dk = 2$, $dr = 0.1$, and k weight $= 1$. Table 2 shows the fitting results of each sample measured after dehydration and partial reduction. All dehydrated fresh C10 Co-MCM-41 catalysts have a first shell Co−O coordination number around 4, suggesting tetrahedral coordination of Co with surrounding oxygen ions created by the isomorphous substitution of Si ions. The bond length between Co and oxygen of Co-MCM-41 is longer than that of $CoAl_2O_4$, probably due to the distortion of tetrahedral coordination by the substitution of the Si ion with Co, which has a larger ionic radius than Si. The degree of distortion, therefore, may increase as a function of pH because the Co/Si molar ratio increases as pH increases, as discussed above; a continuous increase of the Co−O bond length is shown in Table 2. When these catalysts were partially reduced at 700 °C for 30 min under flowing hydrogen, the low pH adjusted samples started to show a metallic feature in the XANES, and the first-shell Co−Co coordination number could be obtained as shown in Table 2. As expected in the TPR experiment, the reduction stability is increased as the initial pH increases, resulting in decreasing metallic Co−Co coordination number. Reduction at 700 °C of the samples synthesized at high pH, pH >12, was not sufficient

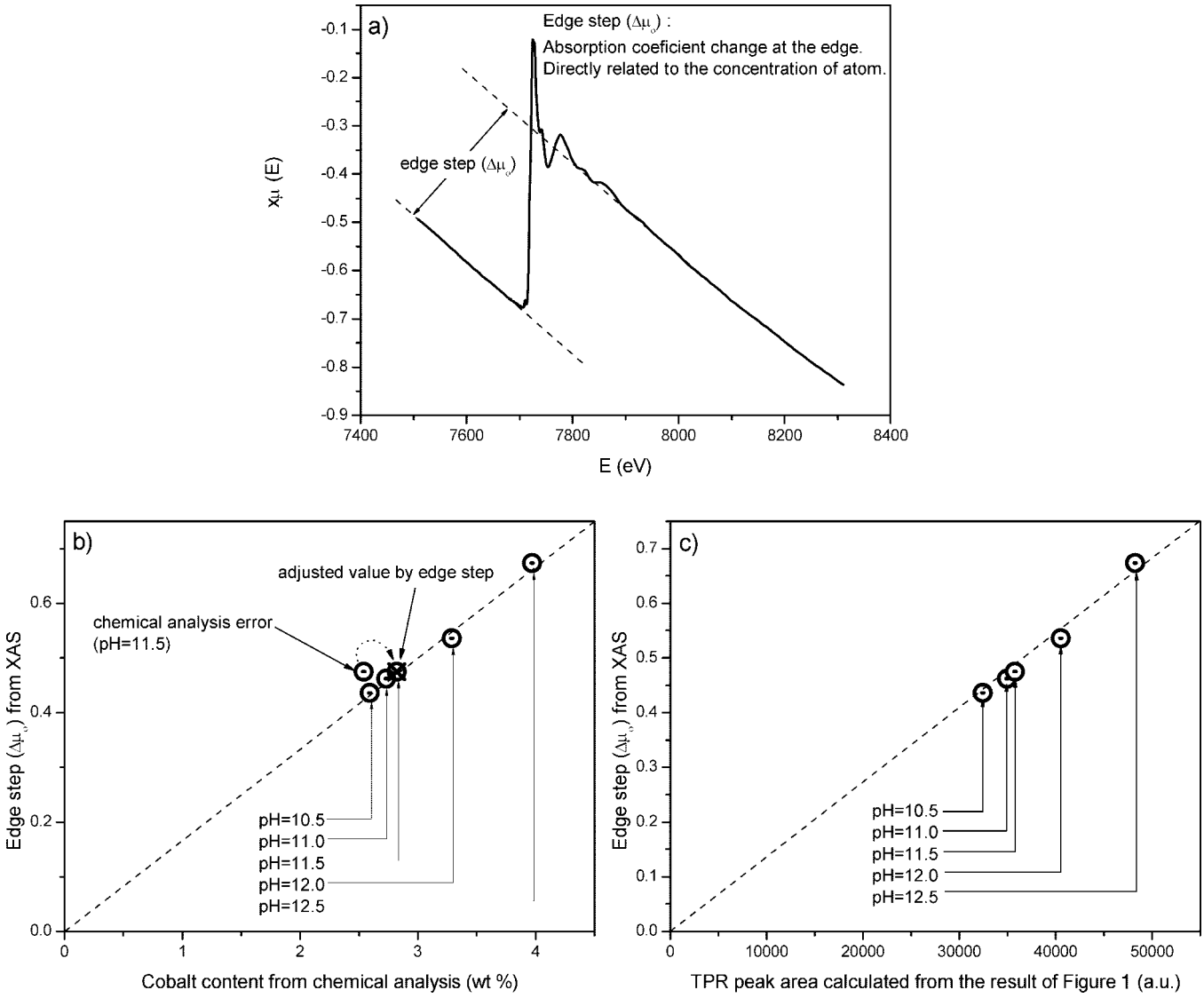

Figure 2. Correlation between the edge step obtained from XANES and the chemical analysis result: (a) typical non-normalized XANES of C10 Co-MCM-41 showing the edge step, (b) plotting the edge step with the chemical analysis result, and (c) plotting the edge step with the TPR peak area from Figure 3.

to obtain a measurable metallic Co−Co coordination number, which indicates that these catalytic systems are highly stable against reduction. Although the Co−Co coordination numbers of the samples synthesized at pH 11 and 11.5 do not show any difference, this may not mean that these two samples have the same of metallic Co cluster size. Apparently, the bond length between Co and Co decreases as pH increases, which suggests that the particle size or, more likely, particle morphology has changed. The EXAFS experiment is insensitive to polydispersity of cluster sizes. The size can be underestimated when different sizes of clusters coexist on the surface.[18,19] Therefore, the contradiction in the particle size prediction made from coordination number and bond length may be due to the polydispersity of cluster size on the surface of the sample synthesized at pH 11. Although these coordination numbers are normalized by total Co amount in the sample, the proper normalization would be by the metallic Co portion only (obtainable by the degree of reduction), the metallic particle sizes obtained here are subnanometer, and these small clusters may be anchored to the surface by bonding to unreduced or partially reduced Co ions maintaining the stability against severe reduction conditions, as discussed earlier.[20]

SWNT Synthesis with C10 Co-MCM-41. The synthesis of SWNT with C10 Co-MCM-41 catalysts prepared in this study was performed by CO disproportionation at different reduction and reaction temperatures to investigate the catalytic behavior related to SWNT quality and yield. Previously, we had reported the catalytic behavior of C16 Co-MCM-41 in the SWNT synthesis, showing a narrow tube size distribution with high selectivity to the SWNT.[7,8] However, the yield of SWNT was limited to about 5 wt % regardless of Co content of the catalyst, indicating every Co was not contributing to the SWNT production. Therefore, if we are capable of increasing the effectiveness of Co without serious aggregation, there would be a good chance to improve the SWNT yield. In this study, we chose a smaller pore size Co-MCM-41 (C10 templated) that showed higher reduction stability than C16 and completely incorporated Co in the silica matrix, resulting in improved control of catalytic active Co particle size and/or morphology.

Because of the different reduction stabilities between C10 and C16 Co-MCM-41, which can result in different optimum reaction conditions, three different reduction/reaction conditions were applied to C10 3 wt % Co-MCM-41, synthesized under the initial pH of 10.5, to monitor the catalytic behavior. As

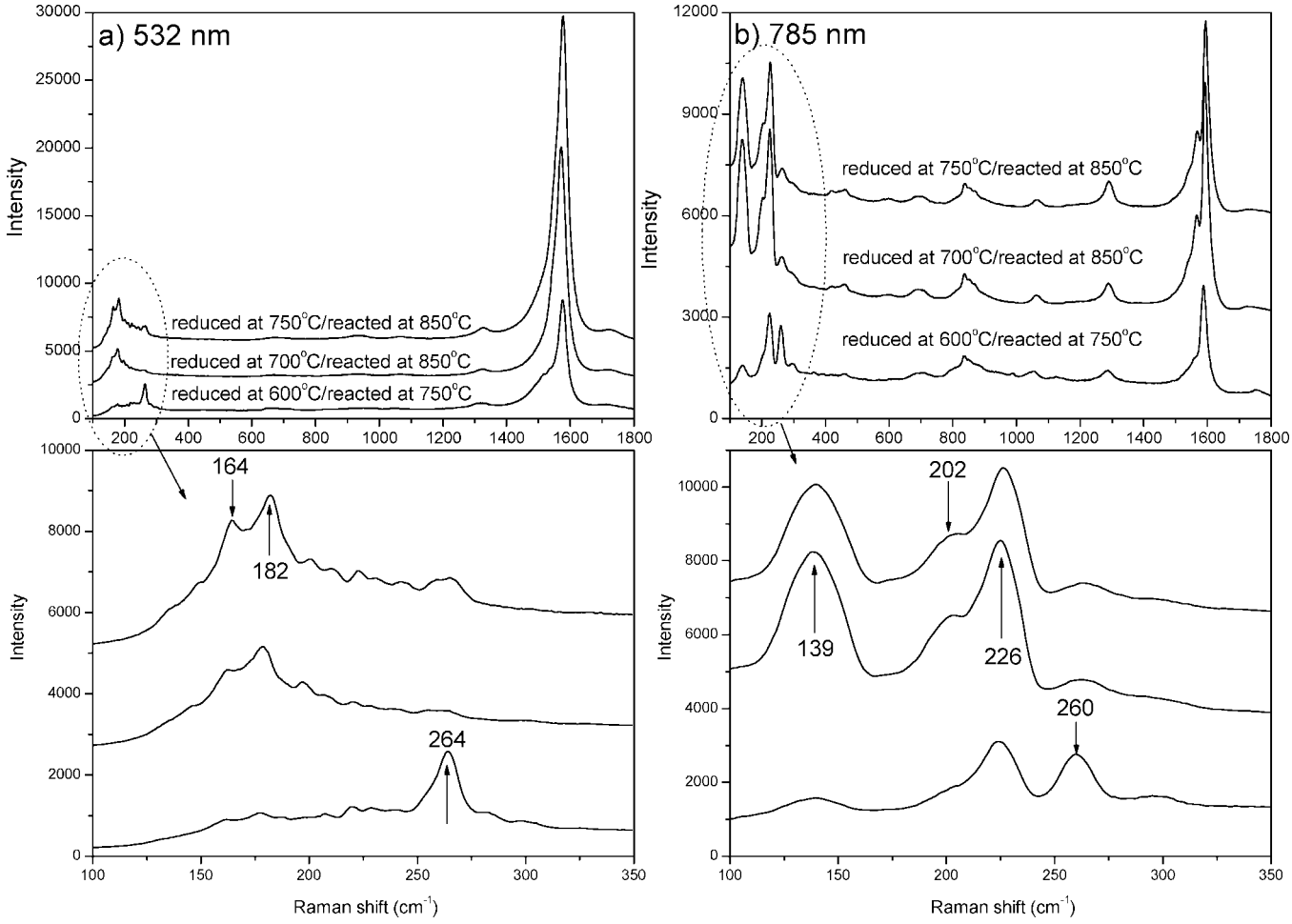

Figure 3. Raman spectra of the unpurified single-walled carbon nanotubes (SWNT) produced under the different reduction and reaction temperatures with C10 Co-MCM-41 catalyst synthesized at the initial pH 10.5: (a) excitation energy = 532 nm and (b) excitation energy = 785 nm.

TABLE 2: Fitting Results of EXAFS Spectra of the Co-MCM-41 Samples and Cobalt Aluminate

		CN		*R* (Å)	
sample	initial pH	Co−Co	Co−O	Co−Co	Co−O
$CoAl_2O_4$ (tetrahedral)			3.99 ± 0.45		1.909
C10 3 wt % Co-MCM-41 fresh (dehydrated)	10.5		4.02 ± 1.24		1.974
	11.0		4.01 ± 1.39		1.971
	11.5		4.03 ± 1.32		1.982
	12.0		4.24 ± 1.24		1.990
	12.5		4.30 ± 1.30		1.998
C10 3 wt % Co-MCM-41 reduced at 700 °C for 30 min	10.5	1.53 ± 0.91	2.42 ± 0.90	2.500	1.940
	11.0	1.25 ± 1.00	2.86 ± 0.99	2.493	1.975
	11.5	1.26 ± 0.97	2.86 ± 0.99	2.488	1.968
	12.0	trace	3.36 ± 0.83		1.974
	12.5	trace	3.30 ± 0.79		1.962

shown in Figure 3, the Raman spectrum of the carbon deposited on the C10 Co-MCM-41 sample at the low reduction and reaction temperatures used in the earlier work with C16 Co-MCM-41 shows narrower tube size distribution than those of the samples prepared at higher temperatures. This is a Raman result typical of what we could also obtain at low SWNT yield (<5 wt %), resulting from the less bundled SWNT because of the low local SWNT population. At higher reduction and reaction temperature, Raman spectra become broader and show larger peaks in the low wavenumber ranges; this can be seen more clearly at the excitation energy of 785 nm. Higher reduction and reaction temperatures can cause serious migration/aggregation of metallic Co clusters, resulting in different size tubes and graphitic carbon formation lowering total carbon yield. However, these batches showed much higher carbon yields than the mild condition (will be shown in Figure 7), suggesting that the multiple and broad peaks in the Raman may not be solely from the different particle and tube sizes. Many researchers have attributed the broadening of the Raman and near-IR (NIR) spectra to the aggregation of SWNT into bundles.[21–25] Recently, Strano used Raman spectroscopy to elucidate the aggregation state of SWNT.[26] Therefore, we would rather explain the multiple and broad peaks in the Raman spectra of these samples by the relationship between SWNT yield and the Raman spectrum.

Although peak broadening may result from greater SWNT aggregation due to the high yield, one cannot overlook the increase of peak intensity in the larger tube size range (wave-

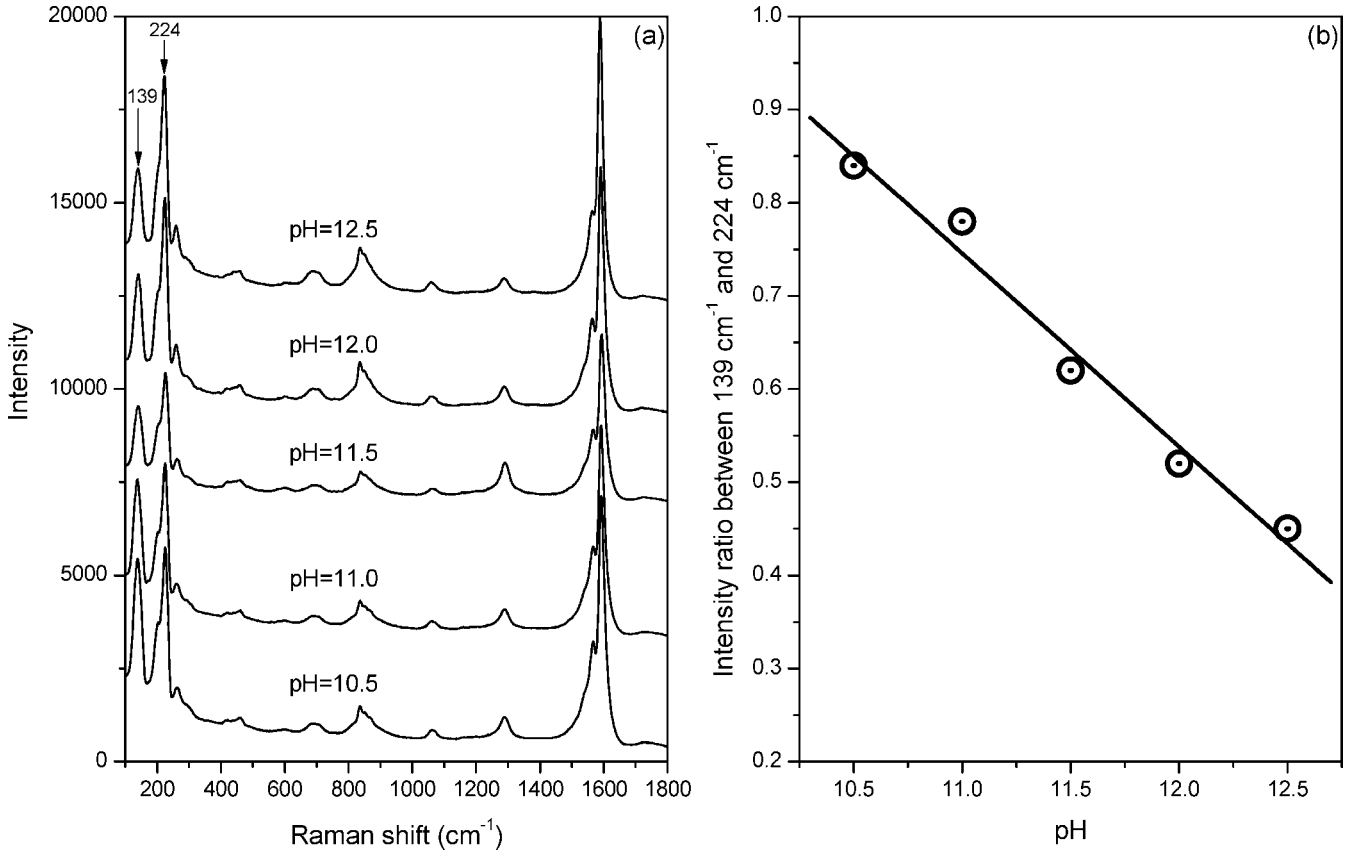

Figure 4. Raman spectra of the unpurified single-walled carbon nanotubes (SWNT) produced by using C10 Co-MCM-41 catalysts synthesized under different initial pH and peak intensity ratio as a function of the initial pH: (a) Raman spectra and (b) peak ratio as a function of the initial pH.

number = 139, 164, 182, 202, and 226 cm^{-1}) at higher reduction and reaction temperatures. Apparently, this indicates that there are higher numbers of large tubes in the sample produced at higher temperature, which may be directly related to the metal migration/aggregation rates at the different temperatures. The metallic cluster migration rate is a function of reduction and reaction temperatures. At low temperature, resulting in partial reduction, the reduced small metallic clusters are anchored to the surface ions, resulting in a smaller average particle size. However, as the reduction/reaction temperatures increase, all unreduced or partially reduced Co ions will eventually be reduced to metal clusters followed by unconstrained migration, resulting in larger particles. In so far as these particles are in the size range for producing SWNT by the dissociation of CO, carbon tubes will grow on these active particles. The correlation between reduction stability and particle sizes is discussed in detail elsewhere.[20]

The reduction stability is also closely related to the initial pH of the Co-MCM-41 synthesis solution.[12] In an earlier section, it has been shown that the reduction stability of C10 Co-MCM-41 was increased with increasing initial pH of the synthesis solution, which suggests that different tube size may be produced under the same reaction conditions based on the above explanation. Figure 4a shows Raman spectra of carbon tubes on the catalyst synthesized with different initial pH. As pH increases, reduction stability increases, and the peak intensity of the large tube size (139 cm^{-1}) decreases, indicating a smaller portion of large tube sizes. The peak intensity ratios between 139 and 224 cm^{-1} are compared in Figure 4b. Surprisingly, these two major tube size ratios show a linear relationship to the initial pH of the Co-MCM-41 synthesis solution. This result strongly suggests that reduction stability is a key factor to control the Co cluster size, which determines the tube size.

Figure 5 shows a typical TG/DTG result of carbon oxidation performed on C10 Co-MCM-41 synthesized under the initial pH 10.5, and reduced and reacted at 700 and 850 °C, respectively, to calculate the carbon yield and roughly separate the different carbon species. By using a deconvolution technique with Gaussian fitting, four different peaks could be separated: amorphous carbon around 300 °C, carbon tubes around 450 and 600 °C, and graphite between 850 and 950 °C. It is not clear why there are two oxidation peaks for carbon tubes. However, one can hypothesize that they result from different tube sizes, bundle sizes, tube locations (inside the pore and on the surface of catalyst), and metal−tube interactions. One of these situations or a combination of these can result in two or more different oxidation temperatures.[27]

If the first peak in Figure 5 is amorphous carbon, the D band of the Raman spectrum will decrease or disappear after oxidation at 500 °C. However, as shown in Figure 6, the Raman spectra obtained before and after oxidation do not show any difference in the D band intensity. The D band probably results from the original defect density of SWNT. This tells us that the first peak of the bimodal peaks is not amorphous carbon. Furthermore, the intensity of RBM peaks after oxidation decreases compared to that of the as-synthesized sample, which indicates that this peak is from SWNT.

The next issue is the origin of the second peak around 600 °C. This might be considered to be MWNT if the first peak is SWNT and we assume each species of carbon gives a single oxidation peak. We cannot observe MWNT with Raman analysis. The first analysis approach can be TEM. Although

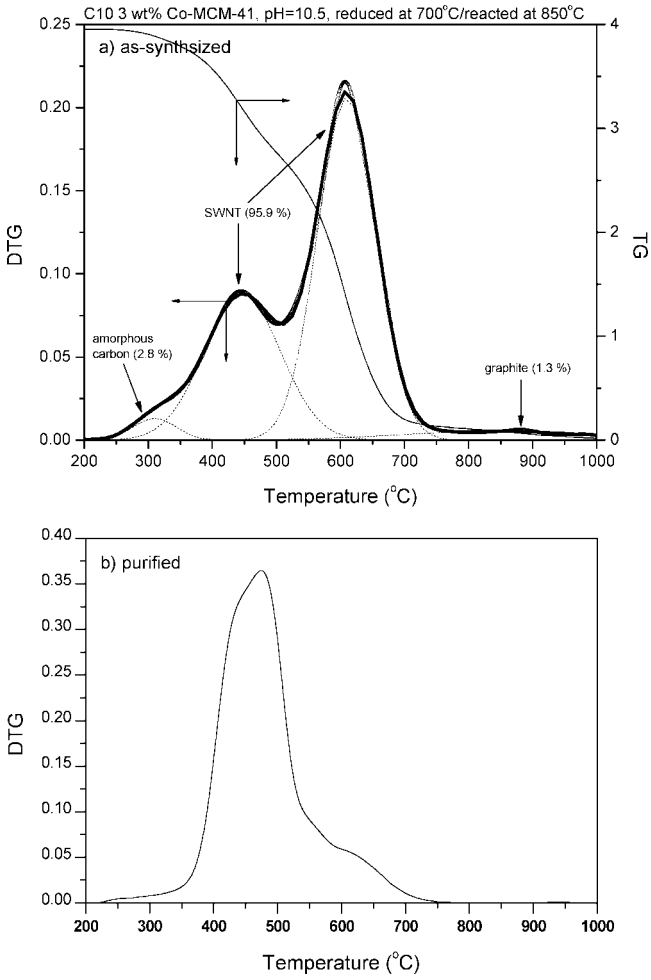

Figure 5. Temperature-programmed oxidation (TPO) result of the unpurified single-walled carbon nanotubes (SWNT) with TG/DTG.

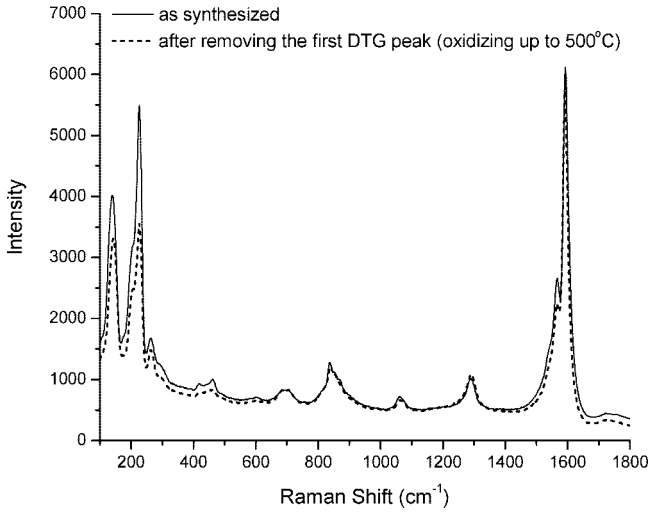

Figure 6. Raman spectra of the unpurified single-walled carbon nanotubes (SWNT) before and after oxidation at 500 °C.

TEM shows only local information, we could not find any MWNT through multiple observations of the as-synthesized sample. Second, graphite and MWNT can be easily recognized by XRD. If the second peak is MWNT, there should be no problem in the detection limit in the XRD analysis. However, we have not seen any diffraction peaks with this sample. Third, when we oxidized the purified sample (after removing silica and Co) with the TG method, there was a dramatic decrease in the second peak intensity, with only a small shoulder remaining in the DTG pattern, see Figure 5b. If the second peak were MWNT (which is more stable with respect to oxidation than SWNT), we should see an intense peak at the same temperature. On the basis of these results, we suggest that the bimodal peaks are both SWNT. The bimodal shape was probably caused mainly by the different bundle size because the second peak mostly disappeared after purification, resulting in an increase of the first peak, which may be attributed to the debundling of SWNT during the purification process consisting of reflux with hydrochloric acid and ultrasonification. The effect of metal-catalyzed oxidation is negligible compared to the bundle size effect because we did not see any peak shift to the higher temperature after purification.

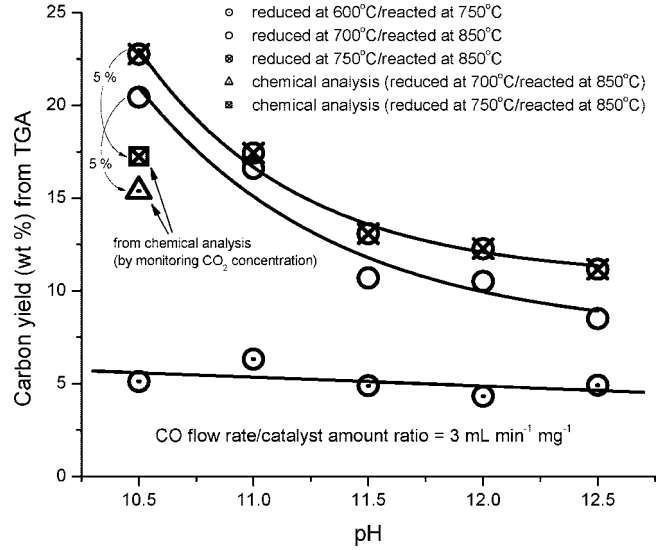

Figure 7. Carbon yield obtained under the different reduction and reaction conditions as a function of the initial pH of the catalyst synthesis solution.

TABLE 3: EXAFS Fitting Result of C10 Co-MCM-41 Samples after Reaction

sample	initial pH	CN Co−Co[a]	CN Co−O	*R* (Å) Co−Co	*R* (Å) Co−O
C10 3 wt % Co-MCM-41 after reaction[b]	10.5	7.46 ± 0.65		2.496	
	11.0	6.59 ± 0.67		2.497	
	11.5	7.48 ± 0.46		2.495	
	12.0	6.84 ± 0.59		2.495	
	12.5	7.31 ± 0.52		2.495	

[a] Corresponds to particle size from 1.2 to 1.4 nm. [b] Reduced at 700 °C/reacted at 850 °C.

Therefore, we assign the two oxidation peaks in Figure 5a as SWNT, and estimate the selectivity of SWNT at about 96 wt %. The oxygen consumption or production by the oxidation of metallic cobalt and cobalt oxide decomposition, respectively, could not be differentiated in the total oxygen consumption, so this sample was sent outside (Galbraith Laboratory, Knoxville, TN) for complementary analysis of carbon yield by CO_2 detection. There was about a 5% (absolute, ~25% change) difference between the TG and CO_2 detection methods, see Figure 7.

Figure 7 shows the carbon yields obtained from different reduction and reaction temperatures with C10 Co-MCM-41 catalysts synthesized under the different initial pH conditions. These results are from the TG experiment for the purpose of relative comparison under the same conditions. There is no

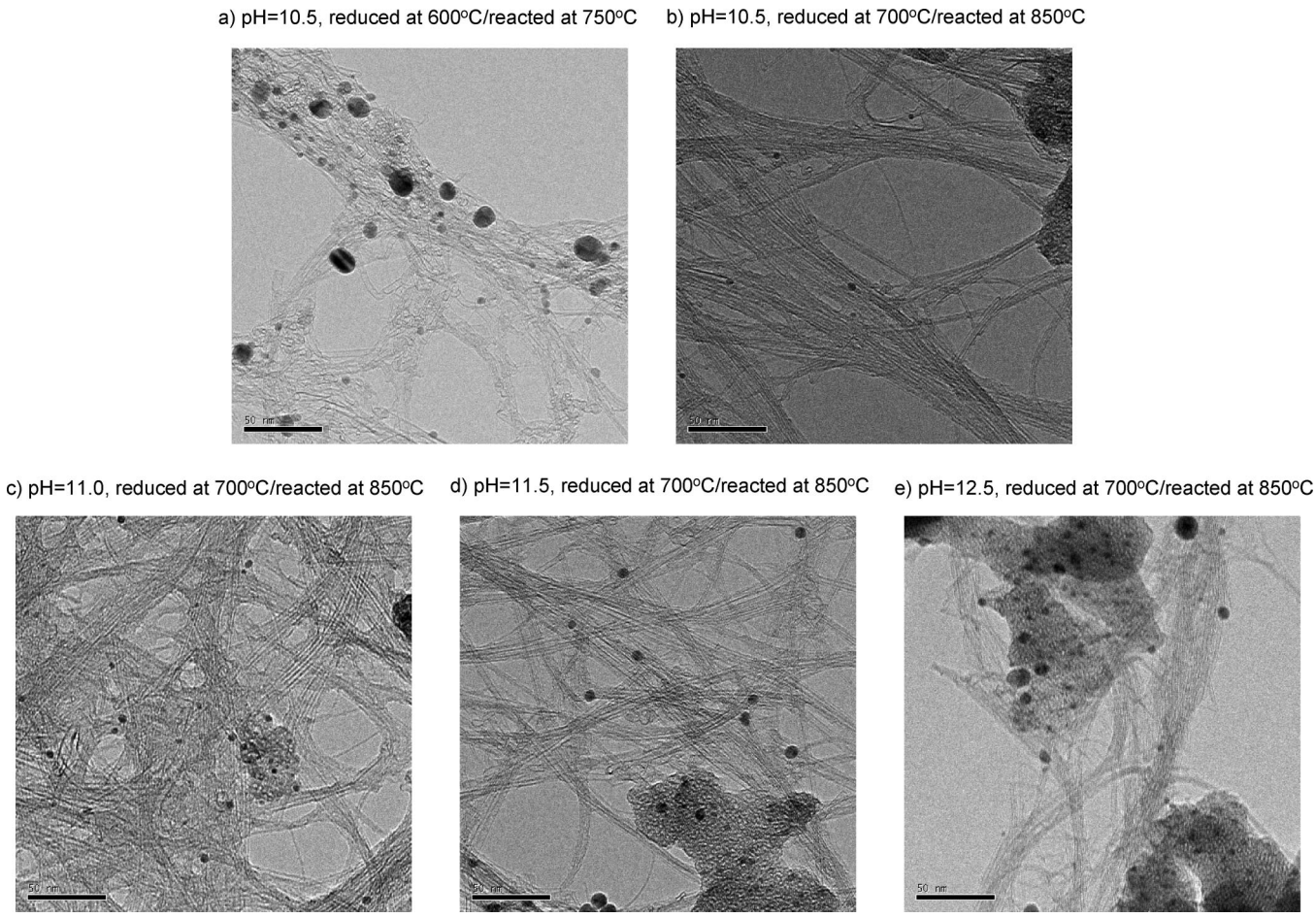

Figure 8. TEM images of the unpurified single-walled carbon nanotubes (SWNT) produced by using C10 Co-MCM-41 catalysts synthesized under different initial pH values.

significant difference in the carbon yield when the catalyst was reduced at 600 °C and reacted at 750 °C, the same conditions as for the optimum for C16 Co-MCM-41 where the carbon yield is around 5 wt %. At this low reduction temperature, it is likely that only surface Co cations are reduced, and we hypothesize that pH affects the stability of subsurface Co cations only. However, when the catalyst is reduced at 700 °C and reacted at 850 °C, the carbon yield dramatically increases as the initial pH decreases, in other words, as reduction stability decreases. By increasing the reduction temperature to 750 °C, additional yield increase is noted. This result indicates that the carbon yield is closely related to the catalyst reduction stability, therefore, reduction temperature. The reduction temperatures, 600, 700, and 750 °C, are below the temperature of maximum reduction rate (770 °C) of C10 Co-MCM-41 with pH 10.5. Therefore, not all Co can be reduced at this reduction temperature, resulting in the different degree of reduction. The more Co^{2+} reduced to metal, the greater probability to initiate the CO dissociation reaction on the metallic cluster surface, resulting in higher carbon yield, assuming the average particle size does not increase. However, one has to consider the higher rate of large particle formation under the higher reduction temperature, resulting in low carbon yield because of graphitic carbon formation on these metallic clusters.

At this point, we may consider a third factor that stabilizes the completely reduced metallic Co clusters on the surface. Previously, we have investigated the anchoring and occlusion effects on the stability of partially and completely reduced metallic clusters.[28] In the Co-MCM-41 catalyst, Co ions are incorporated in the silica matrix and eventually migrate to the surface as reduction progresses. Because the MCM-41 wall is amorphous silica, there could be a high probability of the migration of metallic clusters becoming partially or completely occluded by silica. This occlusion actually stabilizes the metallic clusters, resulting in confinement and reduced migration under severe reduction conditions. Because of the occluded active site surface, the catalytic activity at the early stage of reaction can be lower than that of completely exposed active sites. However, as far as the catalytic stability is concerned, this additional stabilizing effect can be a great benefit for the catalyst lifetime.

In the case of the SWNT synthesis, the active site stability is a crucial factor for producing high-quality SWNT with high yield, and we believe the unique property of Co-MCM-41, partial occlusion of metallic cluster particles, contributes to the high yield of SWNT after a higher degree of reduction. Once CO is adsorbed on the active site at the reaction temperature (850 °C), because of the strong electron donor property of CO,[29] a small portion of partially reduced Co ions are completely reduced, resulting in the particle size range from 1.2 to 1.4 nm, obtained by EXAFS analysis summarized in Table 3. Carbon monoxide may create a transient metal−carbonyl group, which is mobile and volatile. Therefore, if there are more unreduced Co ions, as in the case of high pH, there should be a greater chance for the formation of metal−carbonyl groups, resulting in a migration rate surpassing the CO dissociation rate on the active sites. In this case, there is a higher chance to create unwanted carbon species (i.e., graphite) on the surface, affecting

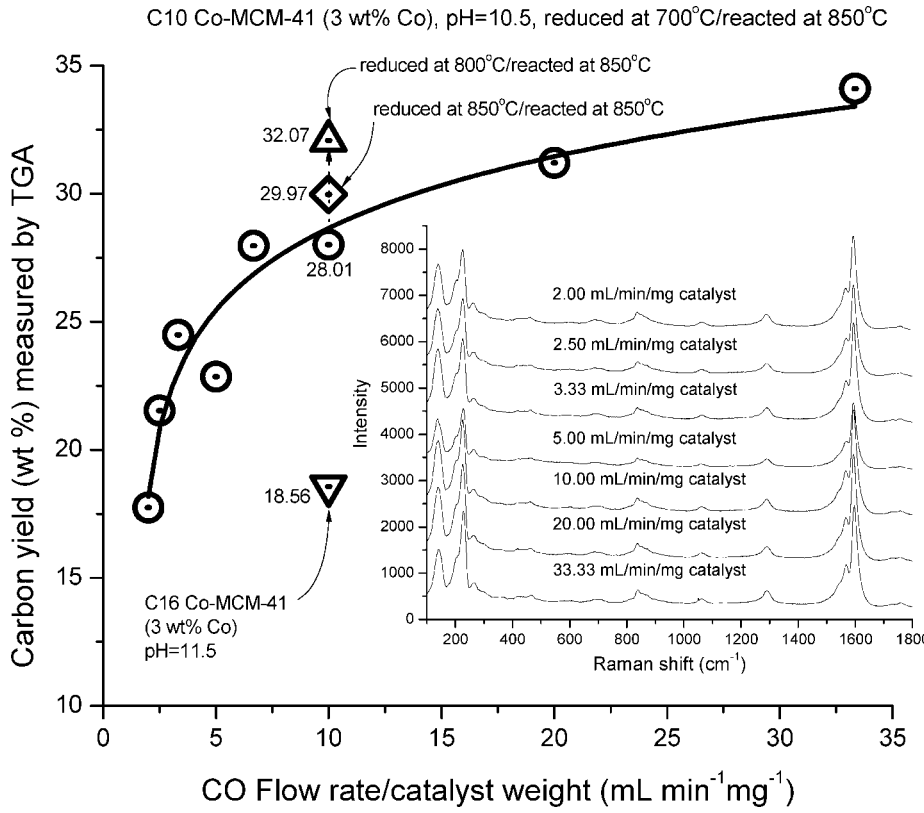

Figure 9. Contact time effect on the carbon yield.

carbon yield and multiple sizes of metallic clusters. This will be a more serious problem at the low reduction temperature, 600 °C. This surmise is clearly shown in the TEM images of reacted catalyst having different pH and reduction/reaction conditions as shown in Figure 8. The sample prereduced at 600 °C shows the largest particle size, and as the initial pH increases, the concentration of metallic clusters increases as well as the size.

To maximize the carbon yield, an engineering study of reaction conditions is a critical component as well as optimizing the catalyst. Many effects of reaction parameters on the SWNT synthesis with Co-MCM-41 catalysts had been investigated systematically in previous work.[7,8] One factor overlooked was the contact time. Because CO disproportionation is a reversible reaction, there can be a high chance of reoxidation of the produced carbon by CO_2 byproduct at low gas flow rate. At the same time, there would be less dissociation of CO on the catalytic active site under the lower partial pressure of CO at the site. The contact time effect, therefore, was investigated by using C10 3 wt % Co-MCM-41 synthesized under the initial pH of 10.5. The reduction temperature and reaction temperature were fixed as 700 and 850 °C, respectively. We chose the reduction temperature as 700 °C, instead of 750 °C which showed higher yield, because we also intended to investigate the reduction temperature effect under the same condition to investigate changes in the carbon yield.

Figure 9 shows the carbon yield changes as a function of contact time (CO flow rate divided by catalyst weight used) along with Raman spectra of these samples after reaction. For this purpose, the CO flow rate was fixed at 1000 mL/min while varying the catalyst amount from 30 mg to 500 mg (CO flow rate/catalyst weight = 2−33.3 mL/(min·mg)). A dramatic increase of the carbon yield with increased contact time at lower times is noted. The maximum carbon yield under these reaction conditions was 34 wt %. The carbon yield was decreased beyond the shortest contact time (not shown here).

The maximum reduction rate temperature of this catalyst was around 770 °C, as discussed in the TPR section. Therefore, if the reduction temperature is increased beyond the maximum reduction rate temperature to reduce Co completely before introducing CO in the reactor to avoid the possibility of carbonyl group formation, that will reduce uncontrolled migration, and the carbon yield may increase further by maximizing the effectiveness (exposure) of Co for the production of SWNT. The unconfined migration to create large particles producing graphitic carbon may not be significant because of the confinement of reduced metallic clusters by occlusion in amorphous silica, as surmised above. There may also be an additional effect of occlusion in the pore itself by the small-pore C10 Co-MCM-41. On the basis of this speculation, one contact time region was selected, and the reduction temperature was increased to 800 °C, which is a higher temperature than the maximum reduction rate temperature of this catalyst. As shown in Figure 9, the carbon yield is further increased, from 28 wt % to 32 wt %, after reduction at 800 °C. This result shows that there may be room to improve the carbon yield above 34 wt % if we use the optimum contact time at this reduction temperature. Further increase of the reduction temperature (850 °C) was not more effective because all Co ions are completely reduced after 800 °C reduction, and there was only slow aggregation of reduced metallic clusters during higher temperature reduction, resulting in less dispersed active sites compared to the sample reduced at 800 °C. However, this prereduction temperature still shows higher carbon yield than that of the sample reduced at 700 °C. This strongly suggests that there is a factor slowing the migration of metallic clusters, which is surmised to be an occlusion effect as discussed above.

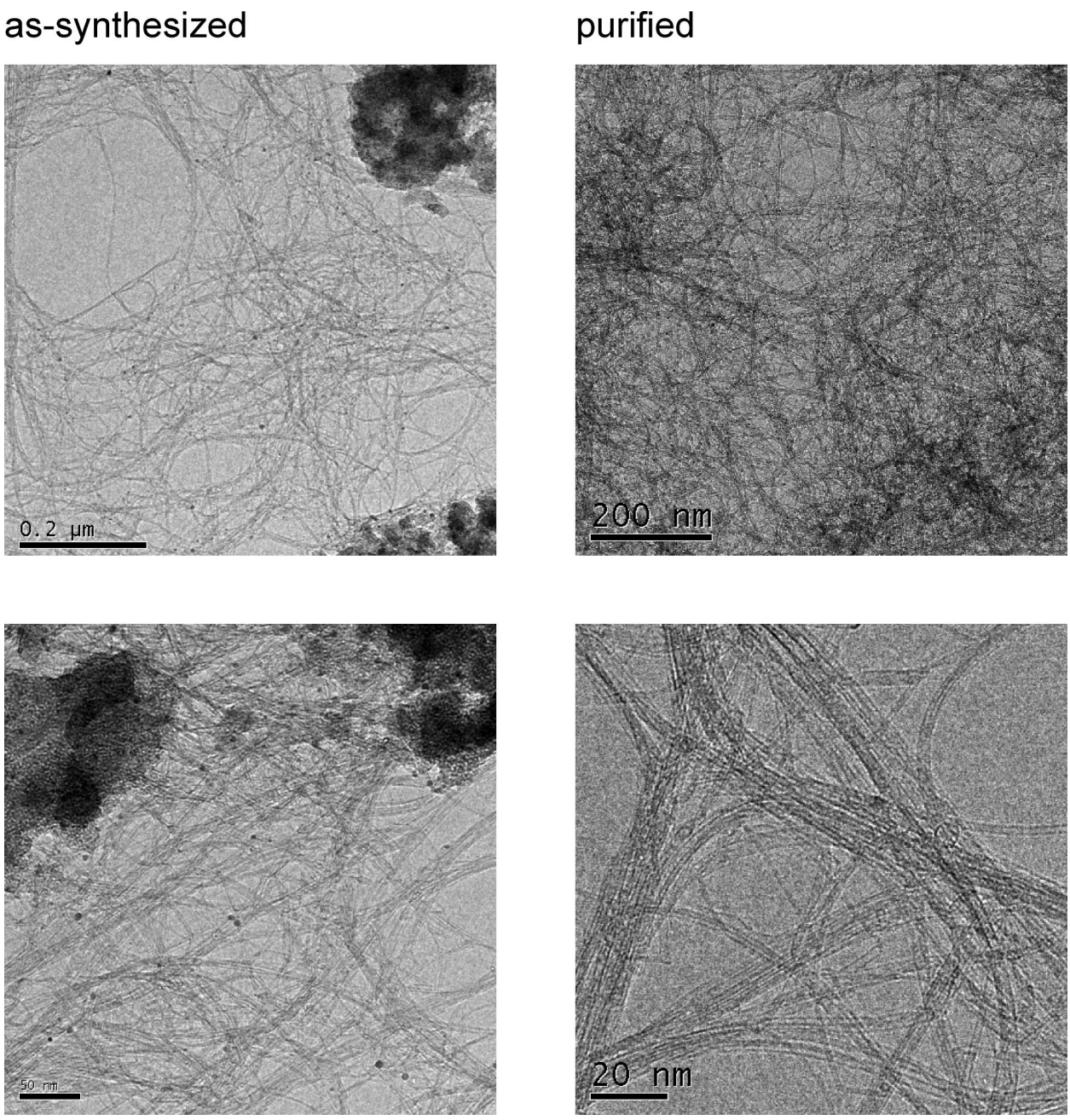

Figure 10. TEM images of single-walled carbon nanotubes (SWNT) before and after purification.

Comparing Co-MCM-41 to the other catalytic systems prepared by impregnation or grafting techniques can be one strategy to explain the benefit of the occlusion effect for the SWNT synthesis catalyst. A 10 wt % Co impregnated MCM-41 and 10 wt % Co grafted SBA-15 (prepared by toluene solution reaction of $Co(acetylacetate)_2$ with surface hydroxyls of MCM-41) were prepared and used for the SWNT synthesis. These two catalytic systems have different reduction patterns: the impregnated one has two major reduction temperature ranges around 300 and 600−850 °C, and the grafted sample has one sharp reduction temperature at 850 °C. Both catalytic systems, therefore, were reduced at 850 °C to completely reduce Co oxides and reacted at 850 °C. The reduced metallic clusters of these two systems are not occluded by silica, unlike C10 Co-MCM-41; therefore, there can be a significant migration on the surface creating large particles, which exceed the particle size required to produce SWNT, resulting in graphitic carbon and lower total carbon yield. TG analysis of these samples after reaction showed the carbon yield at 13 wt % for the grafted sample and below 1 wt % for the impregnated sample yield, values that are far below that of incorporated Co-MCM-41. Both catalysts showed significant amounts of graphite after reaction, produced by large Co particles formed by uncontrolled aggregation on the surface. This result is consistent with an occlusion effect on the stabilization of metallic clusters formed on C10 Co-MCM-41. The C16 3 wt % Co-MCM-41 catalyst was also tested for the complete reduction effect on the carbon yield, as shown in Figure 9. The carbon yield at this condition did not reach the yield of the smaller pore C10 Co-MCM-41, but it shows a higher yield than the grafted sample. From the TPR results earlier, C16 Co-MCM-41 has a small portion of unincorporated surface cobalt oxides reduced around 500 °C, and these surface oxides can form large particles during the temperature increase for the complete reduction of Co, which will produce graphite resulting in lower carbon yield. Therefore, for a proper catalytic system in the SWNT synthesis, all Co

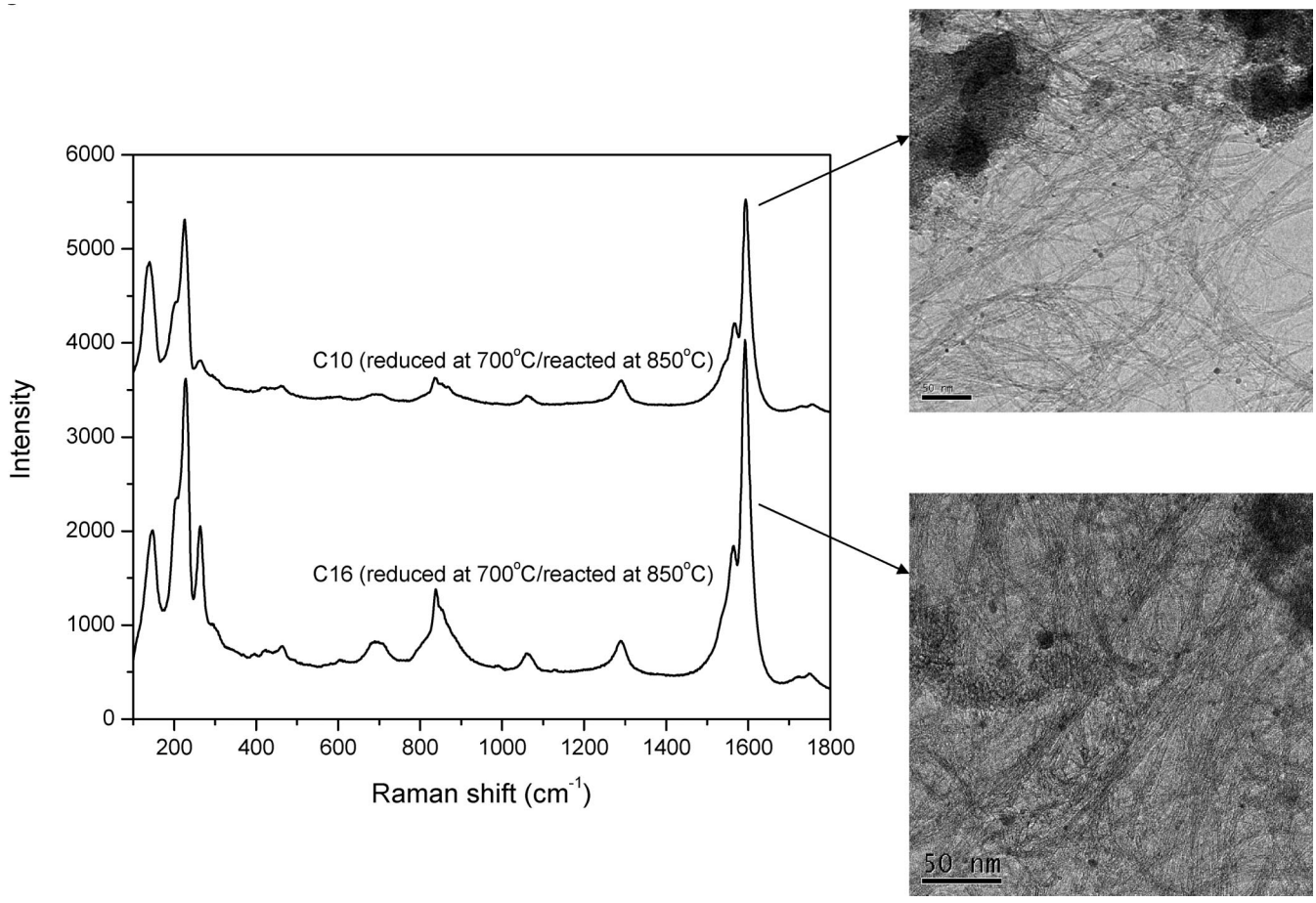

Figure 11. Raman spectra and TEM images of the unpurified single-walled carbon nanotubes (SWNT) produced by using C10 and C16 3 wt % Co-MCM-41 catalysts.

ions have to be completely incorporated into the silica matrix, showing a single and narrow reduction pattern at high temperature. Regardless of the contact time, all samples show the same patterns of Raman spectra, indicating that contact time does not affect the SWNT quality.

Figure 10 shows the TEM images of carbon deposited C10 Co-MCM-41 and SWNT purified by a base−acid treatment.[30] Because of the high yield, the relative metal content is significantly lower compared to that of the sample produced in the earlier work. There is no significant amount of metallic Co clusters observed in the as-synthesized sample. After removing the silica matrix and metallic Co clusters, the image shows only SWNT with high yield and narrow tube size distributions. The purified sample was analyzed by ICP (Galbraith Laboratory, Knoxville, TN), and the metal content was 0.7 wt % in the sample, which is much lower than the 2 wt % obtained from earlier work on C16 Co-MCM-41.

Figure 11 shows the comparison of the Raman spectra and TEM images between C10 and C16 Co-MCM-41 catalysts after carbon deposition under the same reduction and reaction conditions. The C16 sample shows higher density of smaller tube sizes than that of the C10 sample. This can be related to the catalytic system properties, such as the radius of pore curvature effect, which affects the reduction stability, as discussed in the earlier work.[20] Cobalt ions in the large-pore catalyst can be reduced at the lower temperature, and by the time the smaller pore catalyst starts to be reduced, it already forms large particles slowing the migration rate compared to small clusters just formed in the small-pore system. The small particles can migrate faster than large particles formed in the C16 sample, resulting in the larger particles outside the pores in the small-pore system of C10-MCM-41. The particle size is closely related to the tube size; therefore, C16 Co-MCM-41 can produce smaller tube size than C10 Co-MCM-41. Because of the surface Co oxides on the pore walls in the C16 Co-MCM-41 sample, some very large particles and different sizes of metallic clusters could be easily observed compared to the C10 sample, as shown in the TEM images of Figure 11.

The high yield of carbon tubes with high quality (selectivity to SWNT = 96 wt %) may contain a lesser amount of impurities such as amorphous carbon, graphite, metallic residues, and silica. Therefore, there can be a greater chance to recover high-purity SWNT, and this hypothesis was indirectly proved by the nitrogen physisorption experiment. Most surface areas of SWNT reported so far are around 500−600 m^2/g, and our earlier sample (3−5 wt % carbon) showed around 300−400 m^2/g. The SWNT after the final purification (mild oxidation, acid treatment, and reduction) was used for the surface area measurement. Surprisingly, the surface area obtained in this trial showed 1600−1800 m^2/g with the pore volume more than 1 cm^3/g, surpassing the value of the fresh Co-MCM-41 catalyst. These surprising physical properties may result from the high yield and purity, as mentioned above. The pore diameter calculated from nitrogen adsorption analysis is around 0.8 nm. There is a large discrepancy between the tube diameters calculated from the Raman experiment (1.1 and 1.8 nm) and nitrogen physisorption. This discrepancy may result from the tube properties (degree of tube closure, hydrophobic/hydrophilic tube surface, etc.) or inappropriate parameters used in the analysis of the physisorption isotherm. The detailed physisorption study with SWNT is

currently in progress. This extremely high surface area and purity with high yield of SWNT can supply many possibilities of SWNT applications in biomedical engineering, material science, new catalytic support, hydrogen storage, etc.

The carbon yield, in a high area (porous) catalytic process, reported in this study is the highest reported so far, resulting in an increase of purity and quality of SWNT. Although, the factors considered in this report are for one specific catalyst, C10 3 wt % Co-MCM-41, we believe that the hydrogen reduction treatments at the maximum reduction rate to create completely reduced Co and metallic clusters, increasing the effectiveness of the CO disproportionation by minimizing the reduction of unreduced Co ions by CO, which may create transient metal−carbonyl groups and uncontrollable migration, are critical factors in the SWNT synthesis process. This hypothesis needs to be confirmed by further investigation. Different Co-MCM-41 samples without surface Co oxides but having different reduction stabilities need to be investigated to see how such systems behave under the differing reduction treatments. For example, we have only studied C10 samples synthesized at an initial synthesis pH of 10.5, which is the lowest reduction temperature of the C10 series. Higher pH-adjusted samples have higher reduction stabilities. Therefore, the reduction treatment at the maximum reduction rate for each sample may show a similar result to the sample studied in this report. Some of those catalysts have higher temperatures for the reduction than for reaction, which may show completely different results. Also, after complete reduction, using different reaction temperatures may be helpful to understand the reaction mechanism for the SWNT synthesis. The improvement of the catalyst synthesis is a key process component to maximize high-quality SWNT carbon yield, i.e., complete incorporation of metal ions, mild acid washing of surface Co oxides,[10] creation of metal cluster stabilizing forces, etc., may offer other routes to SWNT yield improvement.

Conclusions

Synthesis of high-quality SWNT with high yield was possible by using C10 3 wt % Co-MCM-41. All Co ions were incorporated in the silica matrix, creating a single precursor site Co catalyst and showing high stability against high-temperature reduction. This precisely prepared catalytic system formed nanometer size metallic Co clusters on the surface stabilized by partially occluded amorphous silica during complete reduction. The relative aggregation rate of these stabilized metallic clusters and the CO dissociation rate were balanced such that a high yield of carbon tubes with high purity was achieved. The highest yield obtained in this study was 34 wt %; however, there can be a possible further improvement of the yield by a combination of adjustment of the contact time and the pretreatment conditions. This high-quality SWNT showed very high surface area, 1600−1800 m^2/g, suggesting many possibilities for application of SWNT in various areas. Precise control of the catalytic physical and chemical properties along with reaction parameters are the key to the high-quality SWNT with high yield. It has been found that the catalyst quality and the contact time were the most critical factors to be considered.

Acknowledgment. We are grateful to DoE, Office of Basic Energy Sciences, Grant No. DE-FG02-01ER15183, and DARPA (Hexcel Corp. subcontract) for the financial support of this project.

References and Notes

(1) Lim, S.; Ciuparu, D.; Chen, Y.; Pfefferle, L.; Haller, G. L. *J. Phys. Chem. B* **2004**, *108*, 20095–20101.
(2) Herrera, J. E.; Balzano, L.; Borgna, A.; Alvarez, W. E.; Resasco, D. E. *J. Catal.* **2001**, *204*, 129–145.
(3) Ciuparu, D.; Chen, Y.; Lim, S.; Haller, G. L.; Pfefferle, L. *J. Phys. Chem. B* **2004**, *108*, 503–507.
(4) Hata, K.; Futaba, D. N.; Mizuno, K.; Namai, T.; Yamura, M.; Iijima, S. *Science* **2004**, *306*, 1362–1364.
(5) Cassell, A. M.; Raymakers, J. A.; Kong, J.; Dai, H. *J. Phys. Chem. B* **1999**, *103*, 6484–6492.
(6) Su, M.; Zheng, B.; Liu, J. *Chem. Phys. Lett.* **2000**, *322*, 321–326.
(7) Chen, Y.; Ciuparu, D.; Lim, S.; Yang, Y.; Haller, G. L.; Pfefferle, L. *J. Catal.* **2004**, *225*, 453–465.
(8) Chen, Y.; Ciuparu, D.; Lim, S.; Yang, Y.; Haller, G. L.; Pfefferle, L. *J. Catal.* **2004**, *226*, 351–362.
(9) Barrett, E. P.; Joyner, L. G.; Halenda, P. P. *J. Am. Chem. Soc.* **1951**, *73*, 373–380.
(10) Lim, S.; Ciuparu, D.; Yang, Y.; Du, G.; Pfefferle, L. D.; Haller, G. L. *Microporous Mesoporous Mater.* **2007**, *101*, 200–206.
(11) Amama, P. B.; Lim, S.; Ciuparu, D.; Pfefferle, L.; Haller, G. L. *Microporous Mesoporous Mater.* **2005**, *81*, 191–200.
(12) Lim, S.; Yang, Y.; Ciuparu, D.; Wang, C.; Chen, Y.; Pfefferle, L.; Haller, G. L. *Top. Catal.* **2005**, *34*, 31–40.
(13) Yang, Y.; Lim, S.; Wang, C.; Harding, D.; Haller, G. L. *Microporous Mesoporous Mater.* **2004**, *67*, 245–257.
(14) Stern, E. A.; Newville, M.; Ravel, B.; Yacoby, Y.; Haskel, D. *Phys. B* **1995**, *209*, 117–120.
(15) Pena, M. L.; Kan, Q.; Corma, A.; Rey, F. *Microporous Mesoporous Mater.* **2001**, *44*, 9–16.
(16) Cheng, C. F.; Park, D. H.; Klinowski, J. *J. Chem. Soc., Farad. Trans.* **1997**, *93*, 193–197.
(17) Lim, S.; Ciuparu, D.; Pak, C.; Dobek, F.; Chen, Y.; Harding, D.; Pfefferle, L.; Haller, G. L. *J. Phys. Chem. B* **2003**, *107*, 11048–11056.
(18) Moonen, J.; Slot, J.; Lefferts, L.; Bazin, D.; Dexpert, H. *Phys. B* **1995**, *209*, 689–690.
(19) Bazin, D. C.; Sayers, D. A.; Rehr, J. J. *J. Phys. Chem. B* **1997**, *101*, 11040–11050.
(20) Lim, S.; Ciuparu, D.; Chen, Y.; Yang, Y.; Pfefferle, L.; Haller, G. L. *J. Phys. Chem. B* **2005**, *109*, 2285–2294.
(21) Dresselhaus, M. S.; Eklund, P. C. *Adv. Phys.* **2000**, *49*, 705–814.
(22) Sugano, M.; Kasuya, A.; Tohji, K.; Saito, Y.; Nishina, Y. *Chem. Phys. Lett.* **1998**, *292*, 575–579.
(23) O'Connell, M. J.; Bachilo, S. M.; Huffman, C. B.; Moore, V. C.; Strano, M. S.; Haroz, E. H. *Science* **2002**, *297*, 593–596.
(24) Reich, S.; Thomsen, C.; Ordejon, P. *Phys. Rev. B: Condens. Matter Mater. Phys.* **2002**, *65*, 155411–155411.
(25) Strano, M. S.; Moore, V. C.; Miller, M. K.; Allen, M. J.; Haroz, E. H.; Kittrell, C. *J. Nanosci. Nanotechnol.* **2003**, *3*, 81–86.
(26) Heller, D. A.; Barone, P. W.; Swanson, J. P.; Mayrhofer, R. M.; Strano, M. S. *J. Phys. Chem. B* **2004**, *108*, 6905–6909.
(27) Kitiyanan, B.; Alvarez, W. E.; Harwell, J. H.; Resasco, D. E. *Chem. Phys. Lett.* **2000**, *317*, 497–503.
(28) Lim, S.; Wang, C.; Yang, Y.; Ciuparu, D.; Pfefferle, L.; Haller, G. L. *Catal. Today* **2007**, *123*, 122.
(29) Ciuparu, D.; Chen, Y.; Lim, S.; Ynag, Y.; Haller, G. L.; Pfefferle, L. *J. Phys. Chem. B* **2004**, *108*, 15565–15571.
(30) Chen, Y.; Wei, L.; Wang, B.; Lim, S.; Ciuparu, D.; Zheng, M.; Chen, J.; Zoican, C.; Yang, Y.; Haller, G. L.; Pfefferle, L. D. *ACS Nano* **2007**, *1*, 327–336.

JP710805U